



Published in final edited form as:

Rep U.S. 2021 ; 2021: 6182–6189. doi:10.1109/iros51168.2021.9636180.

Phase-Variable Control of a Powered Knee-Ankle Prosthesis over Continuously Varying Speeds and Inclines

T. Kevin Best,

Department of Electrical Engineering and Computer Science and the Robotics Institute, University of Michigan, Ann Arbor, MI 48109

Kyle R. Embry,

Max Nader Lab for Rehabilitation Technologies and Outcomes Research, Shirley Ryan AbilityLab, and the Department of Physical Medicine and Rehabilitation, Northwestern University, Chicago, IL 60611

Elliott J. Rouse,

Department of Mechanical Engineering and the Robotics Institute, University of Michigan, Ann Arbor, MI 48109

Robert D. Gregg

Department of Electrical Engineering and Computer Science and the Robotics Institute, University of Michigan, Ann Arbor, MI 48109

Abstract

Most controllers for lower-limb robotic prostheses require individually tuned parameter sets for every combination of speed and incline that the device is designed for. Because ambulation occurs over a continuum of speeds and inclines, this design paradigm requires tuning of a potentially prohibitively large number of parameters. This limitation motivates an alternative control framework that enables walking over a range of speeds and inclines while requiring only a limited number of tunable parameters. In this work, we present the implementation of a continuously varying kinematic controller on a custom powered knee-ankle prosthesis. The controller uses a phase variable derived from the residual thigh angle, along with real-time estimates of ground inclination and walking speed, to compute the appropriate knee and ankle joint angles from a continuous model of able-bodied kinematic data. We modify an existing phase variable architecture to allow for changes in speeds and inclines, quantify the closed-loop accuracy of the speed and incline estimation algorithms for various references, and experimentally validate the controller by observing that it replicates kinematic trends seen in able-bodied gait as speed and incline vary.

I. INTRODUCTION

Many activities of daily living require that the knee and ankle joints perform net positive work during the gait cycle, such as walking up stairs or inclines [1]. This presents a

challenge for many people with transfemoral (*i.e.*, above knee) amputations, as most use passive or quasi-passive prosthetic legs that can only store or dissipate energy [2]. Lack of net positive work in the gait cycle can lead to the development of compensatory behaviors [2]–[4], often resulting in fatigue, lower back pain [5] and osteoarthritis [6]. The limitations of conventional prostheses motivate the development of powered prosthetic legs that can perform net positive work and are able to replicate the biomechanical features of normative gait, especially for activities such as stair ascent or incline walking [7].

Despite the potential benefits, there are no fully powered knee-ankle prostheses commercially available today [2], [8]. While advances in actuator technology, energy storage, and robotic limb design have produced systems that are nearly ready for take-home use [9]–[11], the lack of robust and versatile control strategies still limits the viability of these devices leaving the laboratory. State of the art control paradigms [7], [12] typically use discrete controllers for each speed and incline combination (task) and switch between these controllers using a finite state machine (FSM). Each controller requires individually tuned parameter sets for specific periods in the gait cycle (*e.g.*, flat foot, midstance, swing), as well as time or signal thresholds to control transitions between them. In this discrete paradigm, the number of parameters grows quickly as tasks are added to the prosthesis's repertoire. Tuning these parameters is a lengthy process that requires experts in the field [13], making this control architecture potentially less viable for widespread use. In addition, each switching rule introduces an opportunity for the controller to make an incorrect decision, which may increase fall risk for the wearer. Therefore, minimizing the number of switching rules may lead to safer and more clinically viable control methods for powered prosthetic legs.

Recent work has demonstrated promise in transitioning from discrete to continuous control paradigms [14]–[19]. Continuous controllers modulate prosthesis behavior based on analytical rules or models, frequently parameterized by a phase variable. A phase variable represents the user's location in the gait cycle, growing monotonically from 0 to 1 between ipsilateral heelstrikes. It is often defined by a physical kinematic value (*e.g.*, global thigh angle, shank angle) that is readily measured on-board the prosthesis. Many advantages of phase variable parameterizations have been shown, such as an inherent ability to parameterize non-steady gait, robustness against disturbances [20], and backwards walking [16]. Further, continuous controllers have demonstrated the potential to decrease tuning time relative to discrete paradigms, as user gait preferences can be tuned for one task and automatically propagated over the entire task space [21]. The proposed control approach expands upon existing continuous frameworks by adding two more dimensions to the kinematic parameterization: walking speed and ground inclination. This allows a single controller to perform a range of tasks without requiring numerous switching rules and tunable parameters.

It is important to consider whether or not the additional complexity introduced by new parameterization dimensions is offset by a functional benefit for the user. Previous work has shown that while phase variable approaches enable walking over a range of speeds with a single set of kinematic trajectories, biomechanics and energetics are improved when using speed specific kinematics [15]. Further, the joint angles that ensure that the foot

clears the ground during swing and is flat on the ground during midstance depend on the ground incline, suggesting that the kinematic changes in response to incline seen in [22] are important to emulate. Therefore, varying the joint trajectories along task dimensions should produce a more natural gait.

To implement a phase-based controller that generalizes across tasks, we require real-time estimation of walking speed and ground inclination. A previous study [23] used methods similar to [7], [24] to demonstrate that phase, walking speed, and ground inclination can be estimated with sufficient accuracy using only sensors on-board our prosthesis. This work demonstrated speed estimation with 0.06 m/s root mean squared error (RMSE) and incline estimation with 0.52 deg RMSE, which resulted in insignificant errors in the desired kinematic trajectories. However, this previous study did not use the estimated speed and incline values to modify the behavior of the prosthesis in real-time. As shown in Figure 1, the task estimates are part of a feedback loop involving the kinematic model, the joint position controllers, and the user/prosthesis system. To fully understand the online task estimation accuracy and to elucidate any hidden dynamics between the controller components, the full closed-loop system must be tested.

In this work, we present the online implementation of the task estimation algorithms in a continuous, phase-based kinematic controller. We perform human subject treadmill experiments to demonstrate the overall, closed-loop functionality of the task estimators with an adaptive phase variable and a continuous kinematic model. Specifically, this work presents three main contributions: 1) We present modifications to a previous phase variable framework that enables parameterization of the gait cycle over a range of speeds and inclines. 2) We quantify the closed-loop accuracy of the speed and incline estimation algorithms in both steady-state and continuously varying walking activities. 3) We detail and experimentally validate the continuous kinematic control scheme by demonstrating that it produces kinematic trends in response to speed and incline variation that are similar to trends seen in able-bodied gait.

II. CONTROL METHOD

A. Kinematic Model

Embry et al. [22] created a predictive model that represents inter-subject mean kinematics as continuous functions of gait phase s and task $\chi = (\nu, \alpha)$, where ν is the subject's walking speed and α is the ground inclination. This model provides the knee and ankle reference positions for our kinematic controller based on the real-time phase and task estimates. We present a high level overview of the model's construction, but refer the interested reader to [22] for full detail.

Gait kinematics are modeled as the weighted summation of N basis functions of phase, $b_k(s)$. The weight of each basis function changes for each unique task, as determined by the task functions $c_k(\chi)$. This yields the following separable expression for the desired joint angle θ^d of the knee or ankle:

$$\theta^d(s, \chi) = \sum_{k=1}^N b_k(s)c_k(\chi), \quad (1)$$

where the number of basis functions is N , indexed by k . The basis functions are parameterized as finite Fourier series of degree $F=10$, and the task functions are modeled as 2nd or 3rd degree Bernstein basis polynomials. Together, these basis and task functions create a kinematic model $\theta^d(s, \chi)$ that parameterizes how gait cycle phase, speed, and slope affect the joint kinematics.

The model was trained using a kinematic dataset of able-bodied walking with thigh, knee, and ankle angular positions at a variety of phases and tasks. Normalized stride time was used for the phase calculation. The training was formulated as an optimization problem, which was solved using a convex optimization solver like [25] and had a guaranteed globally optimal solution. Able-bodied joint trajectories were chosen for the model because we assume they will produce a more natural gait. We note however that the same method could be used to model any desired kinematic data.

B. Phase Calculation

1) Background: The phase variable is calculated as a piecewise linear function of the residual limb's thigh angle θ_{th} , which can be measured with an inertial measurement unit (IMU) attached to the top of the prosthetic knee hinge as in [16], [17]. The thigh angle trajectory during the gait cycle can be broken into two roughly monotonic sections, where the point of maximum thigh extension defines the transition between sections. We will term the portion of the thigh trajectory between heelstrike and this maximum extension point the *descending* portion, and the remainder of the trajectory the *ascending* portion. For context, the stance to swing transition occurs near the beginning of the *ascending* portion. A finite state machine controls the transitions between portions, detailed in [16]. The phase variable s is defined as

$$s = \begin{cases} \frac{\theta_{th}^0 - \theta_{th}}{\theta_{th}^0 - \theta_{th}^{min}} \cdot c & \text{for } \theta_{th} \text{ descending,} \\ 1 + \frac{1 - s_m}{\theta_{th}^0 - \theta_{th}^m} \cdot (\theta_{th} - \theta_{th}^0) & \text{for } \theta_{th} \text{ ascending,} \end{cases} \quad (2)$$

where θ_{th}^0 and θ_{th}^{min} are the initial and minimum expected thigh angles, respectively. When the phase variable switches from the descending to ascending definition, the current phase s_m and the current residual thigh angle θ_{th}^m are recorded. The constant c defines the phase value at maximum thigh extension and it is tunable based on user preference. We found that our subject's preference for a particular value of c was invariant across speeds and inclines. However if it was found to vary with future subjects, c could likely be estimated in a similar manner as the other phase parameters.

2) Modifications for Varying Tasks: Studies of able-bodied human walking over varying inclines [22] have shown that the maximum and minimum thigh angles during the gait cycle vary significantly with ground inclination. Incorrect estimates of θ_{th}^0 and θ_{th}^{\min} skew the mapping from θ_{th} and s , which results in s arriving at a value other than $s = 1$ at the end of the stride. In these cases, the reference joint angle trajectories produced by the model become unsynchronized with the user's gait, which is undesirable and may result in a fall. Therefore, new algorithms were written to update θ_{th}^0 and θ_{th}^{\min} in real-time as task varies.

During each stride k , the thigh angle at heel strike $\theta_{th}^{HS}[k]$ and the minimum thigh angle observed during stance $\theta_{th}^*[k]$ were recorded. The value of θ_{th}^0 for the upcoming stride was estimated at toe-off as the average of the previous three values of θ_{th}^{HS} :

$$\theta_{th}^0[k + 1] = \sum_{j=0}^2 \frac{\theta_{th}^{HS}[k - j]}{3}. \quad (3)$$

Initial testing with varying tasks showed that this method converged to a steady state value in under five strides and that the user was able to continue a comfortable gait during the convergence period.

However, θ_{th}^{\min} was less straightforward to estimate because it is a function of both the user's intent and the kinematic response of the prosthetic leg. In typical human gait, plantarflexion at the ankle during late stance causes the thigh angle trajectory to reverse directions [26]. Therefore, the timing and value of θ_{th}^* depends on ankle pushoff timing. Because ankle plantarflexion is controlled by the phase measurement, increasing the magnitude of θ_{th}^{\min} shifts pushoff, and thus θ_{th}^* , to occur at larger magnitude hip extensions (2). If a simple average was used to calculate θ_{th}^{\min} , the system would diverge, as each stride would require recursively more hip extension before the ankle would provide pushoff. To prevent this behavior, we instead estimated θ_{th}^{\min} as the maximum (smallest magnitude) of the previous observed values of θ_{th}^* :

$$\theta_{th}^{\min}[k + 1] = \max(\theta_{th}^*[k - j]), 0 \leq j \leq 2. \quad (4)$$

This method proved more effective than an average because it required consecutive strides of increased thigh displacement before decreasing the expected value. Further, in the event that θ_{th}^{\min} was too low, the user could correct it in a single stride by limiting thigh extension.

Finally, the phase estimate was low pass filtered to prevent high frequency changes in the commanded joint positions due to thigh angle measurement noise. A lower cutoff frequency was used during swing ($f_{c, sw} = 4.08$ Hz) than in stance ($f_{c, st} = 13.26$ Hz) because the system is more susceptible to unstable feedback loops (primarily between the thigh IMU and high-bandwidth knee actuator) when the leg is unloaded. The phase filtering had negligible

effect on the kinematics during swing, as toe clearance and an appropriate foot position at heelstrike were still provided.

C. Task Estimation

In addition to the phase measurement, the kinematic model requires knowledge of the user's desired walking speed and the ground inclination, which we term the current *task*. The current task was estimated using on-board sensor information from recent previous strides. The estimates were updated at each toe-off event and filtered with a three-sample moving average to reduce noise.

1) Steady Gait Determination: The task estimation algorithms' objective is to predict the walking speed and ground inclination of the upcoming stride based on information gathered during previous strides. Therefore, we restricted the task estimators to only update during periods of steady gait, as non-steady periods are by definition not representative of the expected task in upcoming strides.

Gait was considered steady if it satisfied the following criteria: 1) The position of the foot relative to the hip was significantly different (20 cm) between each change in ground contact. The foot position was calculated based on known link lengths and forward kinematics. This criteria was intended to discard periods of weight shifting during standing and mid-stride pauses. 2) Heelstrikes occurred at least 0.25 s apart. Any consecutive heelstrikes temporally closer together were discarded, again likely an indicator of standing weight shifting. 3) Heelstrikes occurred no more than 3.0 s apart. This criteria detected when the user had stopped walking. When any of the criteria were not met, the task estimators retained their previous values.

2) Speed Estimation: Speed estimates were based on a double-pendulum model of human walking and utilized measurements of the thigh angle θ_{th} (from the thigh IMU), knee angle θ_k (from the joint encoder), and a priori measurements of the subject's thigh length L_{th} and tibia length L_{ti} , in a manner similar to [24]. Joint angles were defined positively in flexion, relative to the proximal link, and the zero configuration corresponded to quiet vertical stance. The model assumed symmetry and that the distance travelled by the subject during one stride was equal to the summation of the foot's anterior/posterior displacement with respect to the hip during stance and swing. The foot's saggital-plane position with respect to the hip joint center p_{th} is given by

$$p_{th}(t) = L_{th} \begin{bmatrix} \cos(\theta_{th}(t)) \\ \sin(\theta_{th}(t)) \end{bmatrix} + L_{ti} \begin{bmatrix} \cos(\theta_{th}(t) + \theta_k(t)) \\ \sin(\theta_{th}(t) + \theta_k(t)) \end{bmatrix}. \quad (5)$$

The displacements during stance and swing were calculated at every ipsilateral heel strike (HS) or toe-off (TO) event:

$$\begin{aligned} d_{stance} &= \|p_{th}(t_{TO}) - p_{th}(t_{HS}^-)\|_2, \quad \text{if } t = t_{TO}, \\ d_{swing} &= \|p_{th}(t_{HS}) - p_{th}(t_{TO}^-)\|_2, \quad \text{if } t = t_{HS}, \end{aligned} \quad (6)$$

where $t_{\overline{TO}}$ and $t_{\overline{HS}}$ are the times of the previous TO or HS event, respectively. Then at every TO event, the average speed of the stride was updated:

$$v(t) = \begin{cases} (d_{\text{stance}} + d_{\text{swing}})/(t_{\text{HS}} - t_{\overline{HS}}), & \text{if } t = t_{\text{HS}}, \\ v(t-1) & \text{otherwise.} \end{cases} \quad (7)$$

3) Incline Estimation: The ground inclination α was estimated by measuring the angle of the foot with respect to gravity when the foot was flat on the ground (midstance). A similar incline estimation algorithm was presented in [7] on a knee-ankle prosthesis using an accelerometer at the foot and force sensors placed at the heel and the toe. We modified this approach to use the sensors already present on our prosthesis, namely a thigh mounted IMU instead of the foot accelerometer and a load cell mounted to the distal end of the ankle joint in place of force sensors for midstance detection. The global foot angle θ_f was calculated based on the global thigh orientation θ_{th} measured by the IMU and forward kinematics:

$$\theta_f = \theta_{\text{th}} - \theta_k + \theta_a + \theta_f^0, \quad (8)$$

where θ_f^0 represents the angle between the prosthetic foot and the sole of the shoe. The constant value of θ_f^0 was experimentally determined during quiet stance on level ground.

The sagittal-plane component of the center of pressure ℓ_{cop} was used to determine when the user was in midstance. It was calculated using the on-board load cell as

$$\ell_{\text{cop}} = \frac{M_y + F_x \ell_x}{-F_z}, \quad (9)$$

where M_y , F_x , and F_z are the y moment, x force, and z force, respectively, and ℓ_x is the distance from the load cell to the bottom of the shoe. The load cell reference frame is oriented such that the x axis is defined positively from the heel to the toes of the prosthetic foot and the y axis is aligned with the ankle axis of rotation (Figure 2). The calculation for ℓ_{cop} was only performed during stance.

The center of pressure location is a reliable indicator of midstance because it generally increases monotonically and continuously throughout the gait cycle [27] and it encodes information about the foot's interaction with the ground. Preliminary experiments demonstrated that regardless of ground inclination, the foot was flat on the ground when $3.5 \leq \ell_{\text{cop}} \leq 6.0$ cm. Therefore, to estimate the ground inclination, we simply averaged the measured foot angle θ_f for all time steps during a stride in which the midstance condition was met.

D. Joint Position Controllers

The desired joint angles from the kinematic model were enforced using a modified Proportional-Integral-Derivative (PID) controller. The joint torques at the knee τ_k and ankle

τ_a were calculated as functions of the respective joint's desired position (θ_k^d or θ_a^d) and velocity ($\dot{\theta}_k^d$ or $\dot{\theta}_a^d$), with a general equation for the i th joint's torque given by

$$\tau_i = k_p^i(\theta_i^d - \theta_i) + k_i^i \int (\theta_i^d - \theta_i) dt + k_d^i(\dot{\theta}_i^d - \dot{\theta}_i) - b^i \dot{\theta}_i, \quad (10)$$

where k_p^i , k_i^i , and k_d^i are each joint's unique proportional, integral, and derivative gains. The desired joint velocities $\dot{\theta}_k^d$ and $\dot{\theta}_a^d$ were calculated by numerical differentiation of the position references using Savitzky-Golay filters. An additional viscous damping term was added to help stabilize the controller, with damping coefficient b_i . This term helped eliminate vibrations and oscillatory behavior that naturally arose due to the prosthesis's minimal inherent viscous losses [28]. The integral term was included because it allowed for a more compliant heelstrike while still providing adequate pushoff torque. An anti-windup limit of 170 Nm was implemented on the integral terms. The joint torque commands were scaled by the transmission ratio and sent to the low-level torque controllers implemented on the motor drives. The controller gains were tuned once at the beginning of the experiment and held constant thereafter.

III. EXPERIMENTAL TESTING

A. Hardware Implementation

The proposed control method was implemented on the powered knee-ankle prosthesis designed in [28] (Figure 2). The prosthesis features high torque, low impedance actuators (ILM 85 × 26 motor kit, RoboDrive, Seefeld, Germany) with custom 22:1 single-stage stepped-planet compound planetary gear transmissions. The motors are driven by G-SOLO Twitter R80A/80VDC drives (Elmo Motion Control, Petah Tikva, Israel). A prosthetic foot (Ottobock Lo Rider, 1E57) is mounted below a 6-axis load cell (Sunrise Instruments, Nanning, China), which mounts to the distal end of the ankle joint. The control and signal processing code is implemented on a myRIO 1900 (National Instruments, Austin, TX) mounted on the front of the prosthesis. All control code is executed at 500 Hz. Four on-board LiPo batteries (TP870-3SR70, Thunder Power, Las Vegas, NV) connected in series power the prosthesis. The global orientation of the residual thigh is measured using a 3DM-CX5-25 IMU (LORD Microstrain, Williston, VT) affixed to the proximal end of the knee actuator. Motor positions are measured by E5, 3600 cpr optical quadrature encoders (US Digital, Vancouver, WA). Joint velocities are estimated using second-order Savitzky-Golay filters. Finally, an instrumented treadmill (Bertec, Columbus, OH) measures belt speed and ground inclination.

B. Experimental Protocol

The experimental protocol was approved by the Institutional Review Board of the University of Michigan (HUM00166976). An able-bodied subject was fit with the prosthesis and a bypass adapter. A shoe lift was worn on the contralateral leg to ensure equal leg lengths. The subject was an experienced user of the prosthesis and wore a ceiling mounted safety harness. Before trials began, the subject walked at a self selected pace with a 0.0 deg incline while

the control parameters were tuned, including the position controller gains and the phase variable constant c (Table I). Leg segment lengths were measured on the prosthesis side using a tape measure. Note that L_{th} was reduced by 0.10 m to remove a constant bias in the speed estimates observed during initial testing. We hypothesize that this bias was a result of more complex leg geometry introduced by the bypass adapter that was not well captured by the double pendulum walking model. We assume that this modification will be unnecessary when not using a bypass adapter, and plan to verify this assumption in future trials.

The proposed control strategy was tested over a range of speeds and inclines, both at steady-state and during transient task changes. During each trial, the signals on-board the prosthesis were recorded, as well as the true speed and incline measured by the instrumented treadmill. We tested a range of inclines between ± 6.0 deg and a range of speeds between 0.7 and 1.3 m/s. This range was chosen to explore the majority of the task space without approaching the limits of the kinematic model. During all tests, the parameters from the adaptive phase variable algorithm were used in the phase calculation and the online task estimates were used as inputs to the kinematic model, thus providing insight into the full system's closed-loop behavior. A supplemental video of these experiments is available for download.

1. *Steady-State Task Trials:* Five trials were performed to test the incline estimator's closed-loop steady-state accuracy at different inclines. The subject performed two minutes of steady walking at inclines of -6.0 , -3.0 , 0.0 , 3.0 , and 6.0 deg. Each test was performed at a walking speed of 1.0 m/s. Once the incline estimator, speed estimator, and phase variable parameters reached steady-state at each incline, which typically required 2–6 strides depending on the previous task, two minutes of data were recorded. In a similar manner, the speed estimator's steady-state accuracy was tested at a range of five walking speeds. The subject performed two minutes of steady walking at speeds of 0.7, 0.85, 1.0, 1.15, and 1.3 m/s. Each test was performed with a treadmill incline of 0.0 deg. The two minute data collection period again began when the task and phase parameters reached steady-state.
2. *Transient Task Trials:* The transient closed-loop accuracy of the incline estimator was evaluated in four trials of time-varying inclines. All trials were performed at 1.0 m/s walking speed. Once the subject was comfortable at steady-state, data collection began and the incline was increased from 0.0 deg at a rate of approximately 0.18 deg/s to 6.0 deg. The subject continued walking at the new incline for 30 seconds following the ramp. The trial was repeated for incline transitions from 6.0 deg to 0.0 deg, 0.0 deg to -6.0 deg, and -6.0 deg to 0.0 deg. The transient performance of the speed estimate was evaluated in a similar manner. In the first of four trials, the subject walked at 1.0 m/s on a 0.0 deg incline. Once steady-state was reached, data collection began and the treadmill accelerated to 1.3 m/s at a rate of 0.025 m/s². The subject continued walking at the new speed for 30 seconds following the transient. The trial was repeated for speed transitions from 1.3 m/s to 1.0 m/s, 1.0 m/s to 0.7 m/s and 0.7 m/s to 1.0 m/s.

3. *Discontinuous Task Trials:* Four trials were performed to test the robustness of the system to discontinuous changes in task, as well as to characterize the step response of the task estimators. Although the system is not designed to handle discrete changes in task, it is important that it responds safely and converges to the correct state.

In a first test to simulate discontinuous inclines, the subject began walking at 1.0 m/s on a 0.0 degree incline. Once steady-state was reached, the belt speed was quickly stopped and the subject remained stationary while the treadmill was set to a 6.0 degree incline. Once the treadmill reached the correct incline, the belt speed accelerated from 0.0 m/s to 1.0 m/s at a rate of 0.25 m/s² and the subject resumed walking for 30 seconds. The trial was repeated a second time, but instead with a transition to a 6.0 deg decline. Next, to test the system response to discontinuous changes in walking speed, the subject walked at steady-state at 1.0 m/s on a 0.0 degree incline. The treadmill then accelerated to 1.3 m/s at a rate of 15 m/s² to simulate a discontinuous change in speed. The subject continued walking for 30 seconds after the transient change concluded. The trial was repeated a second time, with the treadmill instead decelerating to 0.7 m/s at -15 m/s².

IV. RESULTS AND DISCUSSION

A. Comparisons to Able-Bodied Gait

The proposed control strategy produced kinematic trends in response to task changes that are similar to trends seen in able-bodied gait. First, the phase variable parameter algorithm's output varied as expected with changes in incline (Figure 3), as θ_{th}^0 increased significantly with increasing incline while θ_{th}^{\min} remained relatively constant [22]. This resulted in a consistent phase calculation across inclines.

Next in Figure 4, the average observed joint trajectories for different tasks are plotted as functions of normalized stride time T_0 . The dashed lines show nominal able-bodied trajectories generated from the kinematic model using ideal phase and task estimates. Similar trends appear in both sets of data, such as earlier knee flexion at lower inclines, increased knee and ankle flexion at heelstrike for steep inclines, and increased ankle plantarflexion with increased speed. Further, the observed kinematic trajectories for tasks in the middle of the task space (shallow slopes, moderate speeds) are bounded by the observed kinematic trajectories for the tasks near the edges of the task space (steep slopes, slow and fast speeds), which is also a trend seen in the able-bodied data.

The differences between the observed and nominal kinematics are the net effects of errors in the phase, incline, and speed estimates, imperfect joint position control, and differences in the user's preferred thigh progression relative to the average able-bodied gait. Errors in the phase estimate are the primary contributors to the kinematic discrepancies, manifested as relative time scaling of the trajectories. As seen in Figure 3, the average phase variable does not have a perfectly linear relationship with normalized stride time. Because the kinematic model was fit using normalized stride time, this results in some portions of the observed trajectories appearing faster or slower relative to the nominal trajectories. This problem can be mitigated by re-parameterizing the able-bodied joint trajectories in terms of the average

phase variable instead of normalized time prior to fitting the kinematic model, similar to methods used in [23].

Further, a prominent difference that is notable across all tasks is a slight pause in the kinematic trajectories around 65% of the gait cycle. The pause is due to the phase rate \dot{s} approaching 0 as the thigh reverses directions (Figure 3). Applying the chain rule to (1) and assuming a locally constant task, we can see that θ^d is proportional to \dot{s} :

$$\theta^d(s, \chi) = \dot{s} \sum_{k=1}^N \frac{db_k(s)}{ds} c_k(\chi), \quad (11)$$

and that as $\dot{s} \rightarrow 0, \theta^d \rightarrow 0$. Improving the phase calculation to eliminate this point of zero phase rate would prevent the observed kinematic pause.

Based on these two artifacts, we believe that improving the phase estimates would greatly improve the observed joint trajectories. We plan to investigate modifications to that phase variable that would improve linearity and strict monotonicity while still providing the user with strong volitional control over gait progression.

B. Task Estimator Closed-Loop Accuracy

The closed-loop task estimators were evaluated for their overall steady-state accuracy, low-frequency ramp response, and step response for various task combinations. The steady-state trials demonstrated closed-loop RMSE of 0.041 m/s for the speed estimator and 0.91 deg for the incline estimator during the combined 18 minutes of steady-state walking, shown as functions of task in Figure 5 with error distributions in Figure 6. In addition, the accuracy of the low-frequency ramp response was calculated from the transient task trials (Figure 7) and the errors were similar to the steady-state values. Namely, the speed estimator ramp RMSE was 0.054 m/s and the incline estimator ramp RMSE was 1.36 deg. This modest increase in average error suggests that low-frequency, continuous changes in task do not have an appreciable impact on the task estimators' performance.

We calculated the average error in the commanded joint trajectories that the model would output if the task estimates were biased by their average errors for various task combinations (Table II). The resulting errors of 1 to 2 deg are negligible, especially when compared to the average stride to stride kinematic variation seen in able-bodied subjects [23]. This suggests that task estimators are sufficiently accurate for the purposes of using the kinematic model, and it affirms the prior conclusion that kinematic trajectory discrepancies in Figure 4 are most likely due to phase estimation errors.

Next using the discontinuous task trials, we quantified the task estimate response time, defined as the number of strides required for the estimate to arrive within the bounds of its steady-state accuracy around the true value. For step changes of magnitudes equal to half of the tested task range, the incline algorithm required three strides to converge and the speed algorithm required four strides, on average (Figure 8).

For the discontinuous task changes tested in this study, both estimators converged to the true value in a stable manner and the user was able to continue walking during the convergence period. While this demonstrates that the system is robust to discontinuous changes, it does not however imply that the user would be comfortable or even always be able to continue walking during the transient. For example, it is likely that if the change in task is substantial enough, such as -6 deg to 6 deg, the abrupt change in required kinematics for toe clearance during swing may prevent the user from being able to continue while the task estimator updated. In these cases, a higher-level classifier may be helpful in order to override the task estimates if a discontinuous change was detected.

V. CONCLUSION

This work detailed a continuous, phase-variable control strategy that operated over a continuum of speeds and inclines. The data-driven controller required only a minimal set of tunable parameters that were configured once at level ground walking. We presented an extension to a previous phase variable that allowed it to parameterize the gait cycle over the full task space. We then validated the controller by demonstrating that it replicated kinematic trends seen in able-bodied gait in response to changes in speed and incline. We also quantified the closed-loop accuracy of the task estimators, demonstrating sufficient accuracy for the purposes of using the kinematic model. Further, we demonstrated that the system was robust to discontinuous task changes and that it converged to the true values in less than 5 strides. Finally, we concluded that limitations in the phase variable calculation were the primary cause of discrepancies between the observed and nominal kinematics, suggesting that future work should focus on improving phase estimation.

In future work, we plan to enroll participants with transfemoral amputations to validate this controller's efficacy for a range of individuals. We also plan to explore other applications of the continuous modeling framework, potentially modeling joint impedance and force trajectories as functions of phase and task. Finally, we plan to extend the framework by adding additional dimensions in the task space such as running, stair climbing, and sit-to-stand tasks.

Supplementary Material

Refer to Web version on PubMed Central for supplementary material.

ACKNOWLEDGEMENT

The authors recognize Chris Nesler and Vamsi Peddinti for valuable help with the prototype prosthetic leg and the experiments. They also thank Dr. Edgar Bolívar-Nieto for insightful discussions regarding the phase variable.

This work was supported by the National Institute of Child Health & Human Development of the NIH under Award Number R01HD094772. The content is solely the responsibility of the authors and does not necessarily represent the official views of the NIH.

REFERENCES

- [1]. Grimmer M, Elshamshory AA, and Beckerle P, “Human Lower Limb Joint Biomechanics in Daily Life Activities: A Literature Based Requirement Analysis for Anthropomorphic Robot Design,” *Front. Robot. AI*, vol. 7, no. February, pp. 1–17, 2020. [PubMed: 33501170]
- [2]. Voloshina AS and Collins SH, “Lower limb active prosthetic systems—overview,” in *Wearable Robot*, Rosen J and Ferguson PW, Eds. London, U.K.: Academic Press, 2020, pp. 469–486.
- [3]. Tucker MR, Olivier J, Pagel A, Bleuler H, Bouri M, Lamercy O, Del Millán JR, Riener R, Vallery H, and Gassert R, “Control strategies for active lower extremity prosthetics and orthotics: A review,” *J. Neuroeng. Rehabil*, vol. 12, no. 1, 2015.
- [4]. Gailey R, Allen K, Castles J, Kucharik J, and Roeder M, “Review of secondary physical conditions associated with lower-limb amputation and long-term prosthesis use,” *J. Rehabil. Res. Dev*, vol. 45, no. 1, pp. 15–30, 2008. [PubMed: 18566923]
- [5]. Ehde DM, Smith DG, Czerniecki JM, Campbell KM, Malchow DM, and Robinson LR, “Back pain as a secondary disability in persons with lower limb amputations,” *Arch. Phys. Med. Rehabil*, vol. 82, no. 6, pp. 731–734, 2001. [PubMed: 11387575]
- [6]. Norvell DC, Czerniecki JM, Reiber GE, Maynard C, Pecoraro JA, and Weiss NS, “The prevalence of knee pain and symptomatic knee osteoarthritis among veteran traumatic amputees and nonamputees,” *Arch. Phys. Med. Rehabil*, vol. 86, no. 3, pp. 487–493, 2005. [PubMed: 15759233]
- [7]. Sup F, Varol HA, and Goldfarb M, “Upslope walking with a powered knee and ankle prosthesis: Initial results with an amputee subject,” *IEEE Trans. Neural Syst. Rehabil. Eng*, vol. 19, no. 1, pp. 71–78, 2011. [PubMed: 20952344]
- [8]. Torrealba RR and Fonseca-Rojas ED, “Toward the Development of Knee Prostheses: Review of Current Active Devices,” *Appl. Mech. Rev*, vol. 71, no. 3, pp. 1–22, 2019.
- [9]. Azocar AF, Mooney LM, Duval JF, Simon AM, Hargrove LJ, and Rouse EJ, “Design and clinical implementation of an open-source bionic leg,” *Nat. Biomed. Eng*, vol. 4, no. 10, pp. 941–953, 2020. [PubMed: 33020601]
- [10]. Lenzi T, Cempini M, Hargrove L, and Kuiken T, “Design, development, and testing of a lightweight hybrid robotic knee prosthesis,” *Int. J. Rob. Res*, vol. 37, no. 8, pp. 953–976, 2018.
- [11]. Lawson BE, Mitchell J, Truex D, Shultz A, Ledoux E, and Goldfarb M, “A robotic leg prosthesis: Design, control, and implementation,” *IEEE Robot. Autom. Mag*, vol. 21, no. 4, pp. 70–81, 2014.
- [12]. Lawson BE, Varol HA, Huff A, Erdemir E, and Goldfarb M, “Control of stair ascent and descent with a powered transfemoral prosthesis,” *IEEE Trans. Neural Syst. Rehabil. Eng*, vol. 21, no. 3, pp. 466–473, 2013. [PubMed: 23096120]
- [13]. Simon AM, Ingraham KA, Fey NP, Finucane SB, Lipschutz RD, Young AJ, and Hargrove LJ, “Configuring a powered knee and ankle prosthesis for transfemoral amputees within five specific ambulation modes,” *PLoS One*, vol. 9, no. 6, 2014.
- [14]. Holgate MA, Sugar TG, and Bohler AW, “A novel control algorithm for wearable robotics using phase plane invariants,” *Proc. - IEEE Int. Conf. Robot. Autom.*, pp. 3845–3850, 2009.
- [15]. Quintero D, Villarreal DJ, Lambert DJ, Kapp S, and Gregg RD, “Continuous-Phase Control of a Powered Knee-Ankle Prosthesis: Amputee Experiments Across Speeds and Inclines,” *IEEE Trans. Robot*, vol. 34, no. 3, pp. 686–701, 2018. [PubMed: 30008623]
- [16]. Rezazadeh S, Quintero D, Divekar N, Reznick E, Gray L, and Gregg RD, “A Phase Variable Approach for Improved Rhythmic and Non-Rhythmic Control of a Powered Knee-Ankle Prosthesis,” *IEEE Access*, vol. 7, pp. 109840–109855, 2019. [PubMed: 31656719]
- [17]. Elery T, Rezazadeh S, Reznick E, Gray L, and Gregg RD, “Effects of a powered knee-ankle prosthesis on amputee hip compensations: A case series,” *IEEE Transactions on Neural Systems and Rehabilitation Engineering*, 2020.
- [18]. Mendez J, Hood S, Gunnell A, and Lenzi T, “Powered knee and ankle prosthesis with indirect volitional swing control enables level-ground walking and crossing over obstacles,” *Sci. Robot*, vol. 5, no. 44, 2020.

- [19]. Thatte N, Shah T, and Geyer H, "Robust and adaptive lower limb prosthesis stance control via extended kalman filter-based gait phase estimation," *IEEE Robot. Autom. Lett.*, vol. 4, no. 4, pp. 3129–3136, 2019.
- [20]. Villarreal DJ, Poonawala HA, and Gregg RD, "A Robust Parameterization of Human Gait Patterns Across Phase-Shifting Perturbations," *IEEE Trans. Neural Syst. Rehabil. Eng.*, vol. 25, no. 3, pp. 265–278, 2017. [PubMed: 27187967]
- [21]. Reznick E, Embry K, and Gregg RD, "Predicting Individualized Joint Kinematics over a Continuous Range of Slopes and Speeds," *Proc. IEEE RAS EMBS Int. Conf. Biomed. Robot. Biomechatronics*, vol. 2020–November, pp. 666–672, 2020.
- [22]. Embry K, Villarreal DJ, Macaluso RL, and Gregg RD, "Modeling the Kinematics of Human Locomotion over Continuously Varying Speeds and Inclines," *IEEE Trans. Neural Syst. Rehabil. Eng.*, vol. 26, no. 12, pp. 2342–2350, 2018. [PubMed: 30403633]
- [23]. Embry KR and Gregg RD, "Analysis of Continuously Varying Kinematics for Prosthetic Leg Control Applications," *IEEE Trans. Neural Syst. Rehabil. Eng.*, 2020.
- [24]. Aminian K, Najafi B, Büla C, Leyvraz P-F, and Robert P, "Spatio-temporal parameters of gait measured by an ambulatory system using miniature gyroscopes," *J. Biomech.*, vol. 35, no. 5, pp. 689–699, 2002. [PubMed: 11955509]
- [25]. Grant M and Boyd S, "Graph implementations for nonsmooth convex programs," in *Recent Advances in Learning and Control*. Springer, 2008, pp. 95–110.
- [26]. Perry J, Burnfield J, and Cabico L, *Gait Analysis: Normal and Pathological Function*, 2nd ed. Thorofare, NJ: Slack, 2010.
- [27]. Winter DA, *Biomechanics and Motor Control of Human Movement: Fourth Edition*, 2009.
- [28]. Elery T, Rezazadeh S, Nesler C, and Gregg RD, "Design and Validation of a Powered Knee-Ankle Prosthesis With High-Torque, Low-Impedance Actuators," *IEEE Trans. Robot.*, pp. 1–20, 2020.

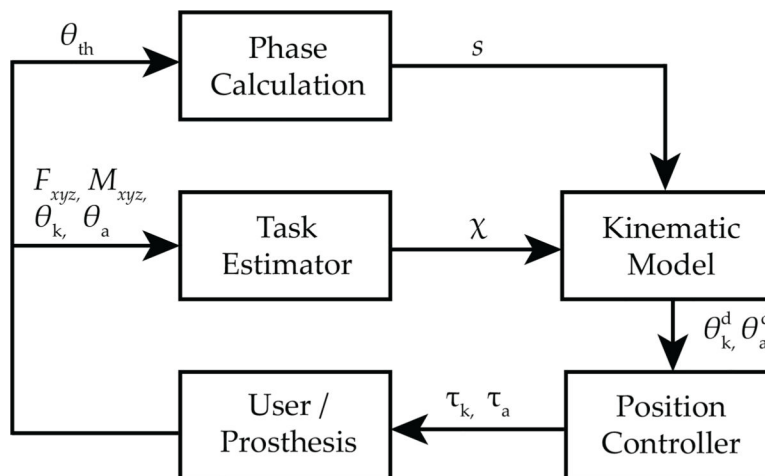


Fig. 1.

A block diagram of the proposed control architecture. A phase estimate s and task estimate χ feed a kinematic model that produces desired knee and ankle reference angles θ_k^d and θ_a^d . A position controller commands knee and ankle joint torques τ_k and τ_a , which interact with the user/prosthesis system to produce thigh, knee, and ankle angles θ_{th} , θ_k , θ_a , and ground contact forces F_{xyz} and moments M_{xyz} .

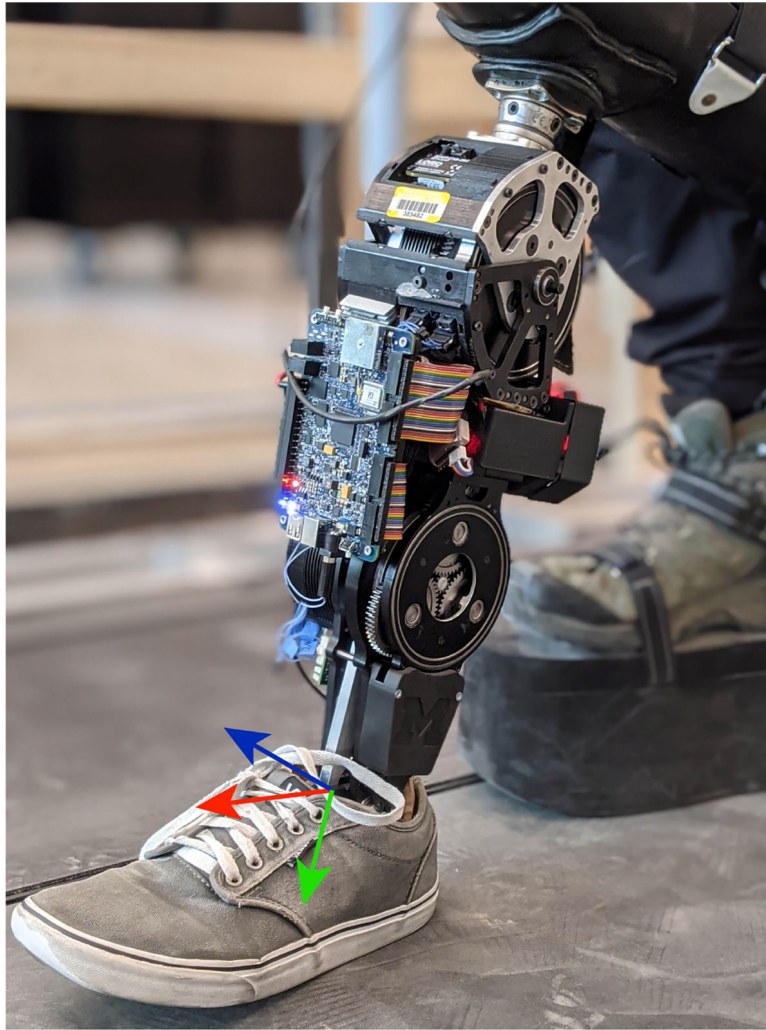


Fig. 2. A photo of the experimental setup, including the custom powered knee-ankle prosthesis attached to the able-bodied subject with a bypass adapter. The load cell x , y , and z coordinate axes are indicated by the red, blue, and green arrows, respectively.

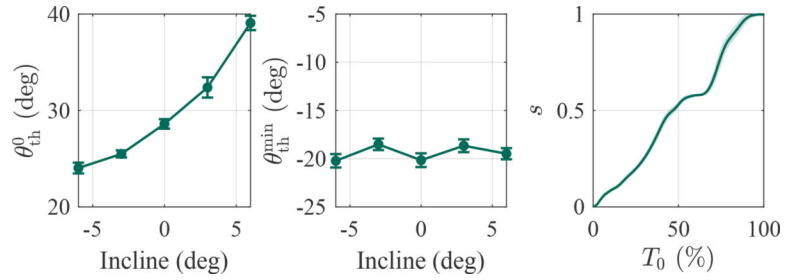
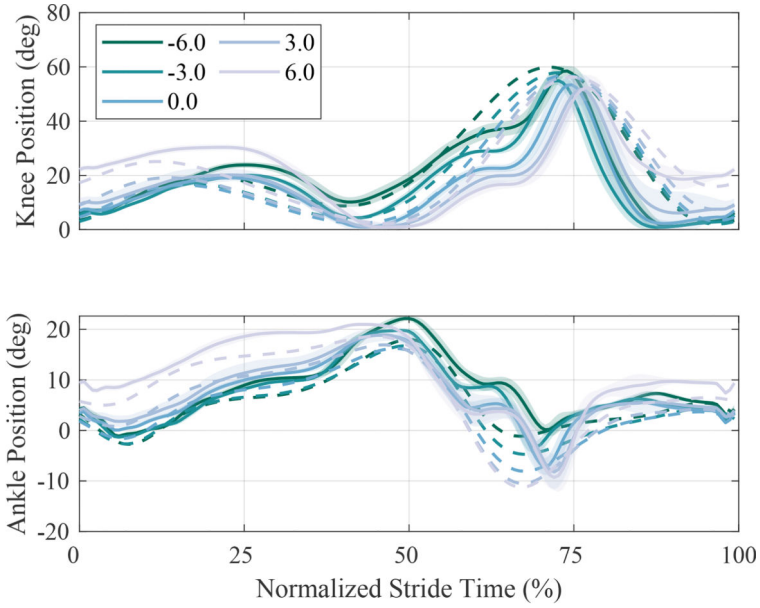
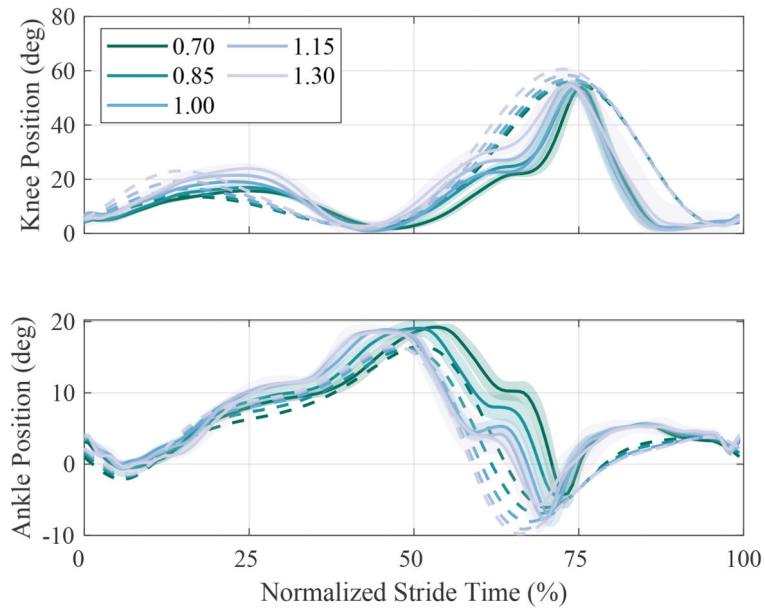


Fig. 3.

The initial (left) and minimum (middle) expected thigh angles produced by the adaptive phase variable parameter algorithm as functions of incline for 1.0 m/s walking. The parameter trends align with observations of able-bodied walking, where θ_{th}^0 increases with incline and θ_{th}^{min} remains relatively constant for the range of inclines tested. The average phase variable trajectory with respect to normalized stride time T_0 (right), with shading representing one standard deviation, shows that modulating these parameters results in a consistent phase calculation that is independent of incline.



(a) Varying inclines (deg)



(b) Varying speeds (m/s)

Fig. 4.

The mean knee and ankle joint angles produced by the prosthesis during the steady-state trials (solid) plotted against the ideal joint angles (dashed) for varying tasks as functions of normalized stride time T_0 . The shaded regions represent one standard deviation on either side of the mean. The changes in kinematics in response to changes in task show trends that resemble trends seen in able-bodied gait. Differences between kinematics are the net result of phase and task estimate errors, and imperfect position control, and user gait individuality.

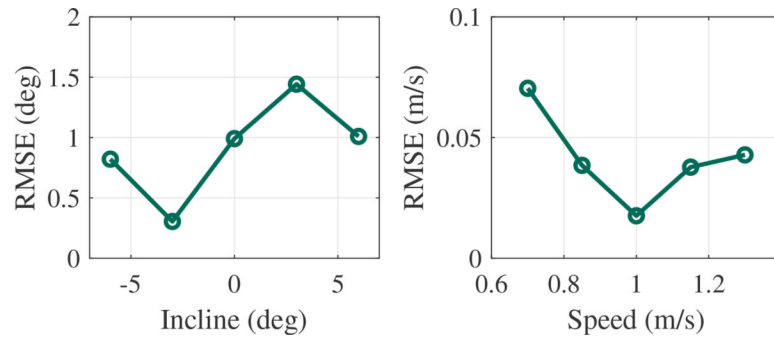


Fig. 5. The RMSE observed in the task estimates during all steady-state walking trials as functions of speed and incline. The average errors over all 18 minutes of steady-state test data were 0.91 deg for the incline estimator and 0.041 m/s for the speed estimator.

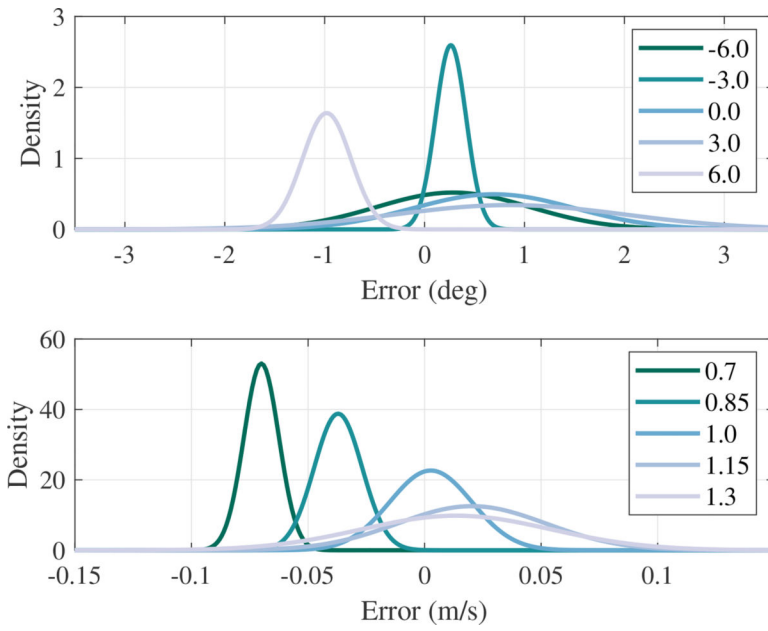


Fig. 6. Normal distributions representing the task estimate errors for different inclines (top) and walking speeds (bottom). The distributions were fit using all 18 minutes of steady-state walking data.

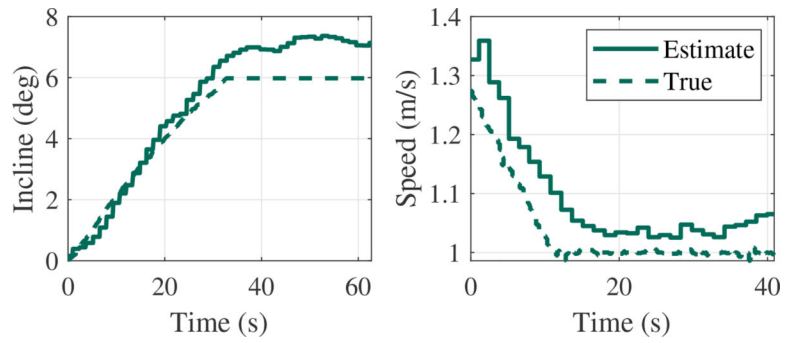


Fig. 7. Example ramp responses of the task estimators during the transient task trials. The left plot shows an incline ramp from 0.0° to 6.0° at 1.0 m/s and the right plot shows a speed ramp from 1.3 to 1.0 m/s at 0.0 deg. These trials indicate that the task estimators can track task ramps in real-time with an accuracy that is similar to steady-state. Note that the piecewise-continuous nature of these plots is due to the estimates updating only once per stride.

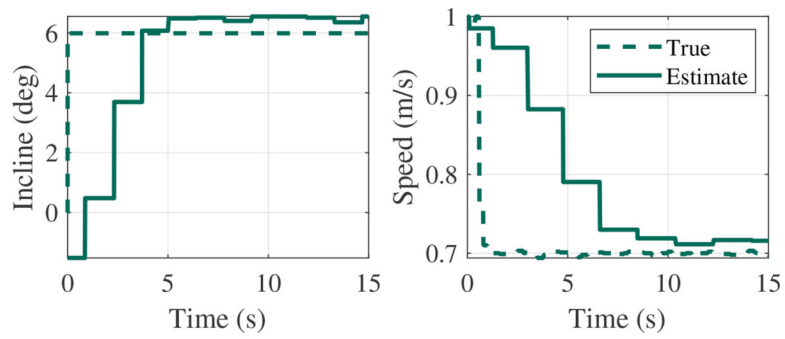


Fig. 8. The step responses of the task estimators during two discontinuous task trials, demonstrating a reasonable response time and robustness to discontinuous changes in task. The left plot shows an instantaneous incline increase from 0.0 deg to 6.0 deg and the right plot shows an instantaneous decrease in walking speed from 1.0 m/s to 0.7 m/s.

TABLE I

Tuned or measured parameters used in all experiments

Parameter	Knee Value	Ankle Value
k_p (Nm/deg)	7.0	15.0
k_i (Nm/deg.s)	0.0	90.0
k_d (Nm.s/deg)	0.05	0.019
b (Nm.s/deg)	0.15	0.056
c	0.58	
θ_f^0 (deg)	0.0	
L_{th} (m)	0.460	
L_{ti} (m)	0.328	

Author Manuscript

Author Manuscript

Author Manuscript

Author Manuscript

TABLE II

Potential joint position errors due to task estimate inaccuracies

Task		RMSE Error (deg)	
True	Potential Estimate	Knee	Ankle
0.0 deg, 1.0 m/s	0.91 deg, 1.041 m/s	0.80	0.74
6.0 deg, 1.3 m/s	5.09 deg, 1.341 m/s	1.51	1.00
-6.0 deg, 0.7 m/s	-6.91 deg, 0.659 m/s	1.56	0.79

Author Manuscript

Author Manuscript

Author Manuscript

Author Manuscript